Inorganic Chemistry

Article

pubs.acs.org/IC

Cooperative Effects of Cation Size and Variable Coordination Modes of Te^{4+} on the Frameworks of New Alkali Metal Indium Tellurites, $NaIn(TeO_3)_2$, $KIn(TeO_3)_2$, $RbInTe_3O_8$, and $CsInTe_3O_8$

Su-whan Bae, Choong-Yeol Kim, Dong Woo Lee, and Kang Min Ok*

Department of Chemistry, Chung-Ang University, 84 Heukseok-ro, Dongjak-gu, Seoul 156-756, Republic of Korea

Supporting Information

ABSTRACT: Four new alkali metal indium tellurites, $NaIn(TeO_3)_2$, $KIn(TeO_3)_2$, $RbInTe_3O_8$, and $CsInTe_3O_8$, have been prepared through hydrothermal and solid state synthesis reactions using corresponding alkali metal carbonates, In_2O_3 [or $In(NO_3)_3{\cdot}xH_2O$], and TeO_2. The structures of the reported materials have been determined by powder and single crystal X-ray diffraction. The mixed indium tellurites reveal a rich structural chemistry with different channel structures. $NaIn(TeO_3)_2$ shows 8-membered rings, whereas stoichiometrically similar $KIn(TeO_3)_2$ exhibits both 8- and 12-membered rings in the frameworks. Isostructural $RbInTe_3O_8$ and $CsInTe_3O_8$ reveal three-dimensional frameworks consisting of InO_6, TeO_3, and TeO_4 groups. Close structural examination suggests that the alkali metal cation size and variable coordination modes of Te^{4+} cations cooperatively influence the framework geometries of the new mixed metal tellurites. Detailed characterizations including spectroscopic, elemental, and thermal analyses are introduced. Local dipole moments and out-of-center distortions for the constituent polyhedra are also reported.

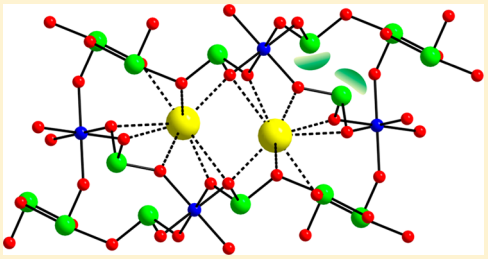

INTRODUCTION

Mixed metal oxides, that is, oxide materials containing two or more metal cations in extended solid state structures have attracted huge attentions owing to their great importance in technological applications such as optics, catalysis, and electric/magnetic properties.[1] The inorganic materials are normally synthesized by solid state, vapor phase transport, and solvothermal methods at higher pressures and temperatures.[2] In order to accurately determine the structures of newly synthesized mixed metal oxides through diffraction techniques, the materials are often prepared in the form of single crystals. Therefore, synthetic chemists have been continuously searching for appropriate methods and proper methods to grow crystals of new compounds. Among many, one of the most versatile starting reagents for the use of crystal growths of novel mixed metal oxides is tellurium dioxide, TeO_2. Attributed to its lower melting point of 733 °C, superior reactivity with unreactive oxide reagents, and excellent solubility in most solvents under moderate reaction conditions, TeO_2 has been widely utilized in the growths of crystals for new oxide materials.[3] Once TeO_2 forms a compound with other metal cations through the reactions, rich structural chemistry revealing a variety of chains, layers, and three-dimensional frameworks has been often observed.[4] The structural variation of mixed metal tellurites may be mainly due to the variable coordination modes of Te^{4+} cations, namely, three-coordinate TeO_3 trigonal pyramids, four-coordinate TeO_4 seesaws, and five-coordinate TeO_5 square pyramids. In addition, as a family of second-order Jahn−Teller (SOJT) distortive cation,[5] the polyhedra of Te^{4+} cation exhibit an unsymmetrical coordination moiety with the lone pair. Thus, many tellurites that are crystallizing in macroscopic non-centrosymmetric (NCS) space groups are frequently observed, and industrially prominent properties such as piezoelectricity, second-harmonic generation (SHG), pyroelectricity, and ferroelectricity are expected from the materials.[6] Another family of cations showing rich framework geometries with its greater flexibility is p-block elements. In particular, when the p-elements are mixed with lone pair cations, various inimitable frameworks could be anticipated in numerous oxide materials with extended structures. We have investigated the discovery of novel mixed metal tellurites in the A^+−In^{3+}−Te^{4+}−oxide (A = alkali metals) system. Although a few indium tellurites[4e,7] as well as indium tellurites halides[8] with a variety of structural features have been reported, to our surprise, only one alkali metal indium tellurium oxide ($Na_{1.4}InTe_{3.6}O_{9.4}$)[7c] revealing a hexagonal tungsten oxide-like layered framework has been reported so far. We were able to discover four new quaternary alkali metal indium tellurites through solid state and hydrothermal reactions. Herein, we present preparations, structure determinations, and thorough characterization of four new quaternary indium tellurium oxides, $NaIn(TeO_3)_2$, $KIn(TeO_3)_2$, $RbInTe_3O_8$, and $CsInTe_3O_8$. We also explain that the cooperative effect of the cation size and variable coordination modes of Te^{4+} plays a key part determining the channel structures of the different tellurites.

Received: August 29, 2014
Published: October 8, 2014

   dx.doi.org/10.1021/ic502108a | Inorg. Chem. 2014, 53, 11328−11334

Table 1. Crystallographic Data for $NaIn(TeO_3)_2$, $KIn(TeO_3)_2$, $RbInTe_3O_8$, and $CsInTe_3O_8$

	$NaInTe_2O_6$	$KInTe_2O_6$	$RbInTe_3O_8$	$CsInTe_3O_8$
fw	489.01	505.12	711.09	758.53
space group	*Pbca* (No. 61)	*Pnma* (No. 62)	$P\bar{1}$ (No. 2)	$P\bar{1}$ (No. 2)
a (Å)	10.673 00(10)	13.3038(2)	5.7616(2)	5.808 10(10)
b (Å)	8.265 00(10)	5.8336(10)	7.5726(3)	7.7458(2)
c (Å)	13.5683(2)	8.2510(10)	11.1342(5)	11.2878(2)
α (deg)	90	90	79.688(2)	79.547(10)
β (deg)	90	90	89.460(2)	89.419(10)
γ (deg)	90	90	70.252(2)	69.380(10)
V (Å^3)	1196.89(3)	640.35(13)	449.15(3)	466.60(4)
Z	8	4	2	2
T (K)	298.0(2)	298.0(2)	298.0(2)	298.0(2)
λ (Å)	0.710 73	0.710 73	0.710 73	0.710 73
ρ_{calcd} (g cm^{-3})	5.428	5.240	5.258	5.399
μ (mm^{-1})	13.542	13.240	17.575	15.581
$R(F)^a$	0.0253	0.0169	0.0328	0.0283
$R_w(F_o^2)^b$	0.0533	0.0426	0.0605	0.0501

$^aR(F) = \Sigma||F_o| - |F_c||/\Sigma |F_o|$. $^bR_w(F_o^2) = [\Sigma w(F_o^2 - F_c^2)^2/\Sigma w(F_o^2)^2]^{1/2}$.

EXPERIMENTAL SECTION

Reagents. Na_2CO_3 (Hayashi, 99.5%), K_2CO_3 (Jin Chemical, 99.5%), Rb_2CO_3 (Acros, 99.5%), Cs_2CO_3 (Aldrich, 99.0%), In_2O_3 (Alfa Aesar, 99.9%), $In(NO_3)_3{\cdot}xH_2O$ (Alfa Aesar, 99.99%), and TeO_2 (Alfa Aesar, 99.99%) were utilized. For further reactions, $AInO_2$ (A = Cs, Rb, K, and Na) were initially synthesized using stoichiometric amounts of A_2CO_3 and In_2O_3 through solid state reactions at 800 °C.

Synthesis. Crystals of $NaIn(TeO_3)_2$ and $RbInTe_3O_8$ were grown through hydrothermal reactions. A 3.00 mmol portion of Na_2CO_3 or Rb_2CO_3, 1.00 mmol of $In(NO_3)_3{\cdot}xH_2O$, 4.00 mmol of TeO_2, and 2 mL of water were put into Teflon lined hydrothermal reactors. The reactors were firmly sealed and heated up to 230 °C, and held for 4 days. After slowly cooling (6 °C h^{-1}) to room temperature, the products were obtained by filtration and rinsed thoroughly with water. Crystals of $NaIn(TeO_3)_2$ and $RbInTe_3O_8$ were isolated in 23% and 34% yields, respectively, based on the corresponding alkali metal carbonates in phase pure forms. Crystals of $KIn(TeO_3)_2$ and $CsInTe_3O_8$, however, were grown through solid state reactions with excess TeO_2 as flux. A 1.00 mmol portion of $KInO_2$ or $CsInO_2$ and 3.00 mmol of TeO_2 were ground well and were transferred into quartz tubes. The tubes were evacuated and sealed under vacuum, and were heated to 350 °C for 5 h, 750 °C (550 °C for $CsInTe_3O_8$) for 48 h, and cooled to room temperature quickly (60 °C h^{-1}). Colorless crystals of $KIn(TeO_3)_2$ and $CsInTe_3O_8$ were obtained with unknown amorphous phases. Bulk phases of pure $NaIn(TeO_3)_2$, $KIn(TeO_3)_2$, $RbInTe_3O_8$, and $CsInTe_3O_8$ were prepared by solid state methods using stoichiometric amount of starting reagents. A 1.00 mmol portion of $AInO_2$ was mixed with 2.00 or 3.00 mmol of TeO_2 and compressed into pellets. The pelletized samples were transferred to silica tubes that were flame-sealed under vacuum. The sealed tubes were heated to 400, 450, and 500 °C (480 °C for $RbInTe_3O_8$ and $CsInTe_3O_8$) for 12 h with intermittent grindings. The bulk products from the reactions were identified as single phases and were in very good agreement with the calculated data from the single crystal X-ray diffraction (XRD) (see the Supporting Information). Although every effort was made to synthesize $RbIn(TeO_3)_2$, $CsIn(TeO_3)_2$, $NaInTe_3O_8$, and $KInTe_3O_8$ at various temperatures with different amount of starting reagents, we were not able to make the materials. In the Supporting Information, a table exhibiting detailed reaction conditions and products was listed. After confirming the thermal properties of $AIn(TeO_3)_2$ (A = Na and K), we also tried stoichiometric reactions between $AIn(TeO_3)_2$ and TeO_2 at 480, 550, and 580 °C for 24 h. However, no substantial changes have been observed from the powder XRD patterns. In addition, heat treatments of $AInTe_3O_8$ (A = Rb or Cs) at 600 °C resulted in the formation of $InTe_3O_8$ and TeO_2 rather than $RbIn(TeO_3)_2$ or $CsIn(TeO_3)_2$, which was also identified by the powder XRD.

Single Crystal XRD. Single crystal XRD was employed to determine the structures of reported materials. A colorless block (0.012 × 0.027 × 0.043 mm^3) for $NaIn(TeO_3)_2$, a colorless block (0.018 × 0.022 × 0.042 mm^3) for $KIn(TeO_3)_2$, a colorless block (0.021 × 0.028 × 0.043 mm^3) for $RbInTe_3O_8$, and a colorless block (0.025 × 0.028 × 0.037 mm^3) for $CsInTe_3O_8$ were used for analyses. The diffraction data were obtained at room temperature with an exposure time of 10 s/frame and scan widths of 0.30° in ω using a Bruker SMART BREEZE diffractometer. The intensities of the obtained data were amended for polarization, air absorption, and Lorentz factor, etc. The programs, SAINT and SADABS, were used for an integration and an absorption correction, respectively.[9,10] The structure solving was obtained using SHELXS-97,[11] while the structure refinement was performed with SHELXL-97.[12] All calculations were carried out using the software package, WinGX-98.[13] Crystallographic data for $NaIn(TeO_3)_2$, $KIn(TeO_3)_2$, $RbInTe_3O_8$, and $CsInTe_3O_8$ are summarized in Table 1.

Powder XRD. The purity of the reported materials was confirmed by powder XRD. The PXRD patterns were recorded on a Bruker D8-Advance diffractometer at room temperature with 40 kV and 40 mA using Cu Kα radiation. The powder samples loaded on glass sample plates were scanned from 10° to 70° in the 2θ range with a step time and a step size of 0.2 s and 0.02°, respectively.

Infrared (IR) Spectroscopy. IR spectral data were collected using a Varian 1000 FT-IR spectrometer with the samples pressed with a KBr matrix in the spectral range 400−4000 cm^{-1}.

UV−Vis Diffuse Reflectance Spectroscopy. UV−vis diffuse reflectance spectra were recorded at room temperature on a Varian Cary 500 scan UV−vis−NIR spectrometer. The absorbance data were transformed from the reflectance spectra.[14]

Thermogravimetric Analysis (TGA). TGA diagrams for the reported materials were obtained with a Setaram LABSYS TG-DTA analyzer to study the thermal stabilities of the materials. Under flowing argon, the loaded samples in alumina crucibles were heated to 1000 °C.

Elemental Analysis. Energy dispersive analysis by X-ray (EDAX) was carried out to determine approximate ratios of elements for the reported materials using a Horiba Energy EX-250. EDAX for $NaIn(TeO_3)_2$, $KIn(TeO_3)_2$, $RbInTe_3O_8$, and $CsInTe_3O_8$ reveal A:In:Te ratios of ca. 1.0:0.9:2.1, 1.0:1.0:1.9, 1.2:1.0:3.2, and 1.0:1.0:2.7, respectively.

dx.doi.org/10.1021/ic502108a | Inorg. Chem. 2014, 53, 11328−11334

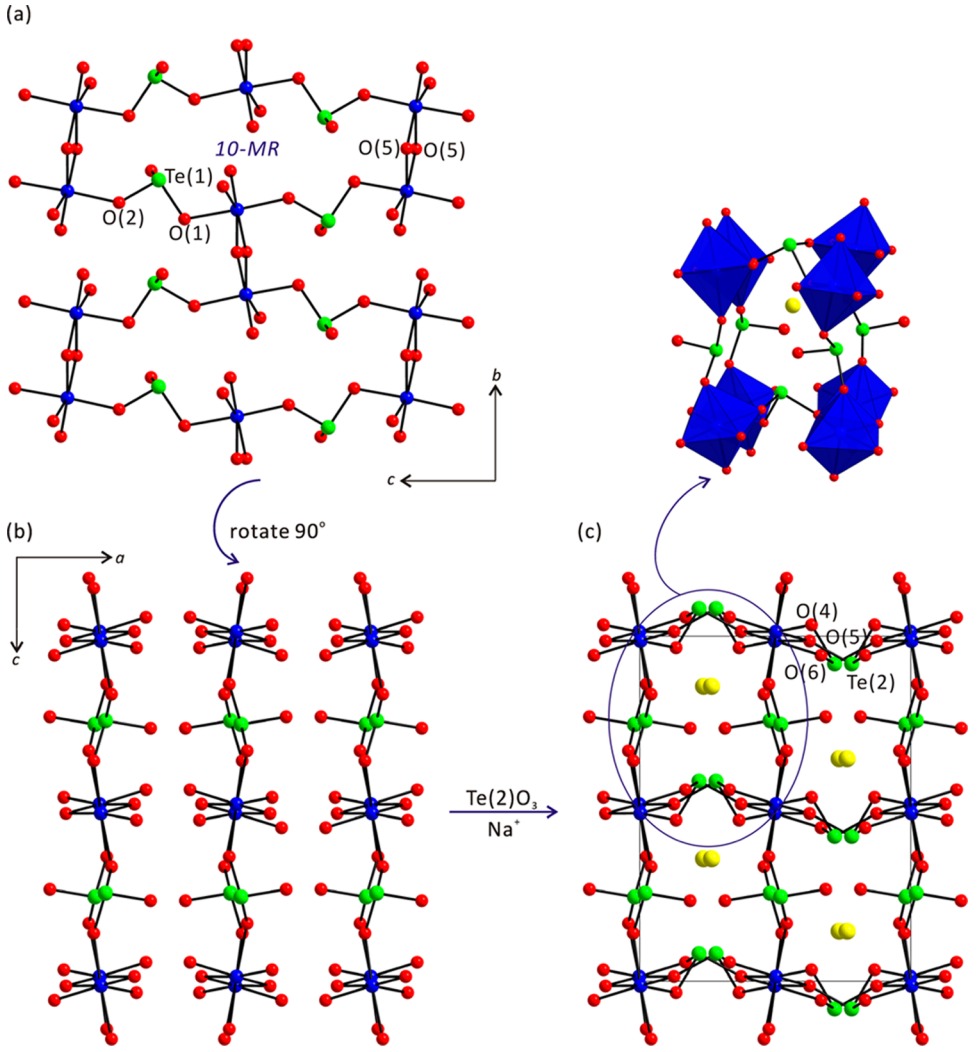

Figure 1. Ball-and-stick models of $NaIn(TeO_3)_2$ representing a layered structure composed of In_2O_{10} dimers and TeO_3 groups (a) in the *bc*-plane and (b) in the *ac*-plane. (c) The layers are connected by $Te(2)O_3$ groups, and a three-dimensional framework is completed (blue, In; green, Te; yellow, Na; red, O).

RESULTS AND DISCUSSION

Structures. $NaIn(TeO_3)_2$. Very little crystallographic information on $NaIn(TeO_3)_2$ has been communicated using the crystal obtained from the reactivity test of $Na_{1.4}InTe_{3.6}O_{9.4}$ in an acidic media.[7c] A more detailed structural description along with full characterization will be given here. The framework of orthorhombic $NaIn(TeO_3)_2$ (space group, *Pbca*) consists of TeO_3 trigonal pyramids and InO_6 octahedra that are connected through oxygen atoms with In−O−Te bonds. The In^{3+} is in a distorted octahedral moiety with the O−In−O bond angles and the In−O bond lengths ranging 77.19(17)−175.68(16)° and 2.107(4)−2.187(4) Å, respectively. Two unique Te^{4+} cations in the structure are linked to three oxygen atoms and generate unsymmetrical trigonal pyramidal environments. The Te−O bond distances in TeO_3 groups range from 1.839(5) to 1.901(4) Å. The Na^+ cations are surrounded by seven oxygen atoms with Na−O contact lengths ranging 2.420(5)−2.970(6) Å. An edge-sharing of two InO_6 octahedra through O(5) form In_2O_{10} dimers. As seen in Figure 1a,b, each In_2O_{10} dimer is linked to $Te(1)O_3$ groups through O(1) and O(2), which makes a layered structure in the *bc*-plane. Ten-membered rings (10-MRs) composed of $In(1)O_6$ octahedra and $Te(1)O_3$ trigonal pyramids are found in the layer. $Te(2)O_3$ groups further link the layers along the [100] direction through O(4), O(5), and O(6) and complete a three-dimensional framework (see Figure 1c). Na^+ cations dwell in the channels of $NaIn(TeO_3)_2$. The structure of $NaIn(TeO_3)_2$ can be represented as an anionic backbone of $\{[In(1)O_{4/2}O_{2/3}]^{-2.333}[Te(1)O_{2/2}O_{1/1}]^{0}[Te(2)O_{2/2}O_{1/3}]^{+1.333}\}^{-}$ in connectivity terms, and the charge balance is retained by the Na^+ cation. Bond valence sums[15] for the Na^+, Te^{4+}, and In^{3+} are calculated to be 0.77, 3.82−4.01, and 3.08, respectively.

$KIn(TeO_3)_2$. Another centrosymmetric material, $KIn(TeO_3)_2$ (space group, *Pnma*), reveals a similar framework structure to that of $KIn(SeO_3)_2$.[16] The new quaternary indium tellurite consists of slightly distorted InO_6 octahedra and TeO_3 groups with In−O−Te bonds. While the In−O bond lengths range from 2.135(3) to 2.176(2) Å, the O−In−O bond angles are in the range 86.49(12)−175.96(13)°. The Te^{4+} is bonded to three oxygen atoms in trigonal pyramidal environments with the Te−O bond distances 1.8528(19)−1.875(3) Å. The K^+ cations interact with eight oxygen atoms with K−O contact lengths of 2.773(2)−2.9755(7) Å. As seen in Figure 2a, discrete InO_6 octahedra share all of the oxygen atoms with TeO_3 polyhedra. At the same time, the TeO_3 groups also share all oxygen atoms

dx.doi.org/10.1021/ic502108a | *Inorg. Chem.* 2014, 53, 11328−11334

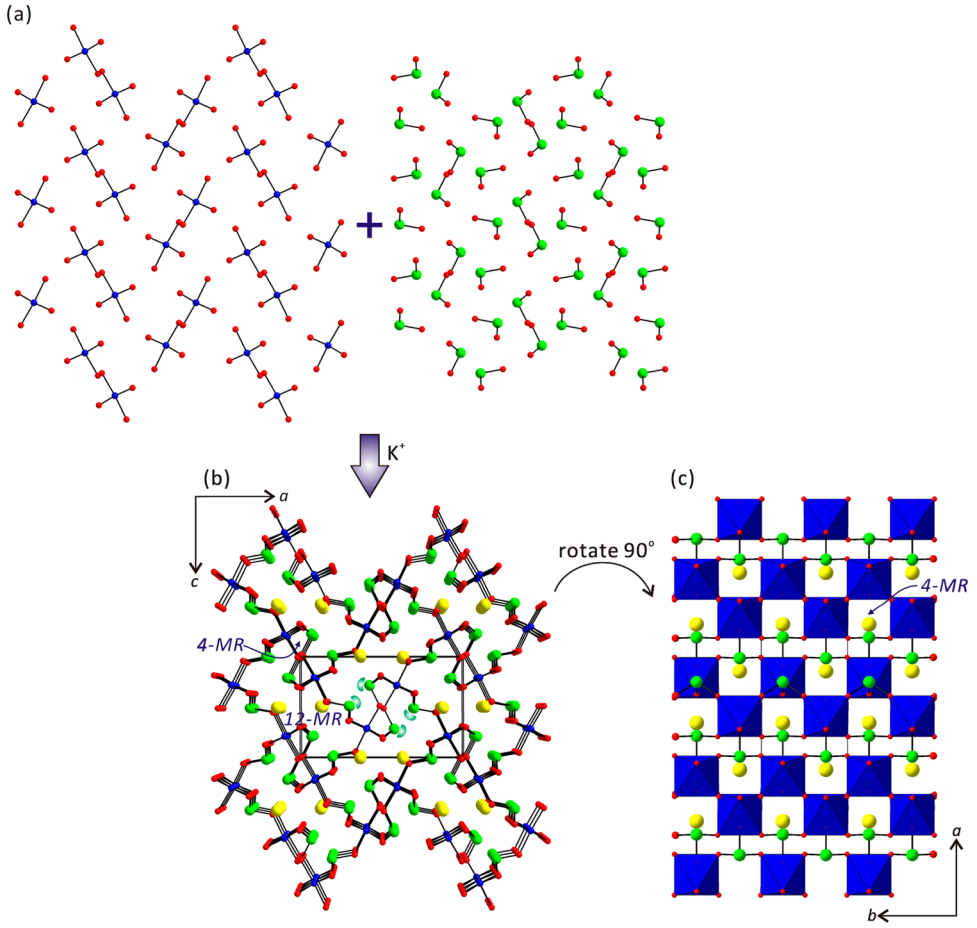

Figure 2. Ball-and-stick and polyhedral representations of $KIn(TeO_3)_2$ (blue, In; green, Te; yellow, K; red, O). (a) Discrete InO_6 octahedra and TeO_3 polyhedra share their oxygen atoms. (b) Small 4-membered ring and large 12-membered ring channels are observed along the [010] direction in the *ac*-plane. Lone pair on Te^{4+} is drawn schematically and not the result of the electron localization function (ELF) calculations. (c) 4-membered ring (4-MR) channels running down the [001] direction are observed in the *ab*-plane.

with InO_6 octahedra and complete a 3D framework. Within the framework, two distinct channels, i.e., 4- (4-MR) and 12-membered ring (12-MR) channels, that are composed of InO_6 and TeO_3 groups, are found along the [010] direction (see Figure 2b). It should be noted that lone pairs on the TeO_3 groups point inward in the larger 12-MR rather than in the smaller 4-MR channels based on the coordination environment of Te^{4+}.[17] K^+ cations also reside in the 12-MR channels, where huge spaces are available. As can be seen in Figure 2c, another 4-MR channel running down the [001] direction is occurring in the *ab*-plane. The structure of $KIn(TeO_3)_2$ in connectivity terms may be written as an anionic framework of $\{[InO_{6/2}]^{-3}\text{-}2[TeO_{3/2}]^{+1}\}^{-}$ with charge balance retained by the K^+. Bond valence sums[15] for the In^{3+}, Te^{4+}, and K^+ are calculated to be 3.03, 4.06−4.14, and 1.14, respectively.

$RbInTe_3O_8$ and $CsInTe_3O_8$. New alkali metal indium tellurites, $RbInTe_3O_8$ and $CsInTe_3O_8$, crystallize in the centrosymmetric space group, $P\bar{1}$. Since $RbInTe_3O_8$ and $CsInTe_3O_8$ are isostructural to each other, only the structural details of $RbInTe_3O_8$ are fully described here. $RbInTe_3O_8$ exhibits a 3D framework consisting of InO_6, TeO_3, and TeO_4 groups with In−O−Te and Te−O−Te bonds. The observed bond distances and angles of In−O and the O−In−O around two unique In^{3+} cations range from 2.140(5) to 2.183(5) Å and from 85.78(17) to 180.0(4)°, respectively. In an asymmetric unit, three unique Te^{4+} cations exist, where the $Te(1)^{4+}$ cation connected to four oxygens is in a seesaw coordination environment, while the $Te(2)^{4+}$ and the $Te(3)^{4+}$ are in three-coordinate trigonal pyramidal modes with three oxygens. However, attributed to the lone pairs, all three unique Te^{4+} cations are in unsymmetrical coordination moieties. The Te−O bond lengths range from 1.860(4) to 2.159(5) Å. The Rb^+ cation is surrounded by nine oxygens with Rb−O contact lengths of 2.816(5)−3.450(5) Å. A novel layer is generated in the *ac*-plane by corner-sharings of $In(1)O_6$ octahedra and $Te(3)O_3$ polyhedra through O(6), O(7), and O(8) (see Figure 3a,b). As seen in Figure 3b, 4-MRs and 8-MRs are obtained from the connections of $In(1)O_6$ octahedra and $Te(3)O_3$ polyhedra within the layer. In addition, a very interesting Te_4O_{10} tetramer is formed, in which an edge-sharing of two $Te(1)O_4$ polyhedra through O(3) and two corner-sharings between $Te(2)O_3$ and $Te(1)O_4$ polyhedra are observed (see Figure 3c). Then, the Te_4O_{10} tetramers serve as interlayer inkers and result in a 3D backbone (see Figure 3c,d). In the *bc*-plane, smaller 5-MR and larger 12-MR channels along the [100] direction are monitored. Since larger Rb^+ cations reside within the 12-MR channels, the lone pairs on the TeO_3 groups point within the smaller 5-MR channels. The structure of $RbInTe_3O_8$ may be considered as an anionic framework of $\{[InO_{6/2}]^{-3}[TeO_{4/2}]^{0}2[TeO_{3/2}]^{+1}\}^{-}$ in connectivity terms, and the overall charge is balanced by the Rb^+ cation sitting in the 12-MR channels. Bond valence sum calculations[15] for the Rb^+,

dx.doi.org/10.1021/ic502108a | *Inorg. Chem.* 2014, 53, 11328−11334

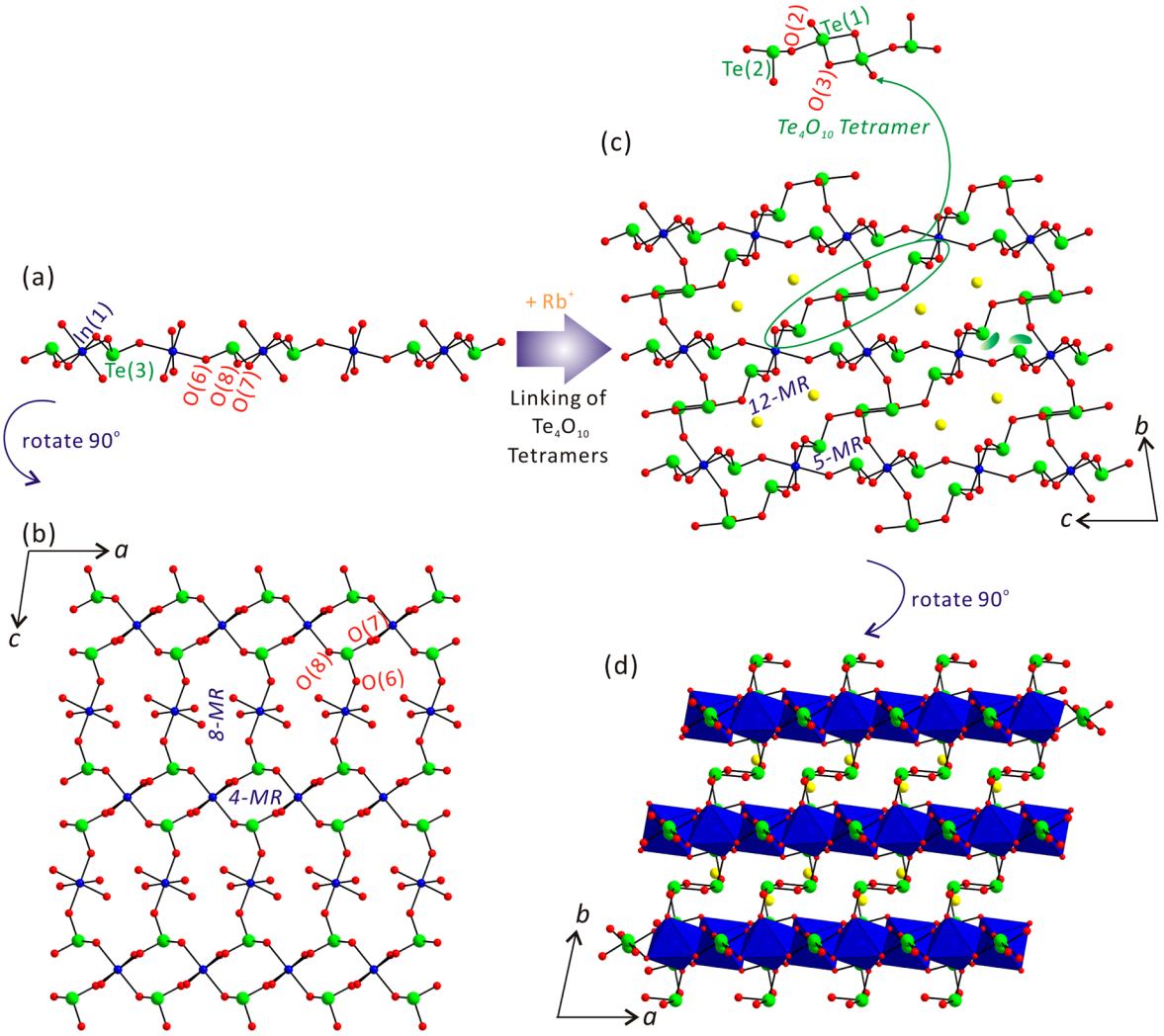

Figure 3. Ball-and-stick and polyhedral representations of $RbInTe_3O_8$ (blue, In; green, Te; yellow, Rb; red, O). (a) $In(1)O_6$ octahedra and $Te(3)O_3$ polyhedra share their corners and generate a layer. (b) 4- and 8-membered rings are observed in the layer. (c and d) Te_4O_{10} tetramers serve as interlayer linkers and form a three-dimensional framework structure.

In^{3+}, and Te^{4+} reveal values of 0.83, 2.93−2.95, and 3.87−3.96, respectively.

IR Spectroscopy. The IR spectra of $NaIn(TeO_3)_2$, $KIn(TeO_3)_2$, $RbInTe_3O_8$, and $CsInTe_3O_8$ show vibrational peaks of In−O and Te−O bonds. Multiple peaks found in the region between 607 and 791 cm^{-1} may be attributable to the Te−O vibrations, and bands observed between 419 and 481 cm^{-1} are due to the In−O vibrations. The assignments of vibration bands show good agreement with those previously reported materials (see the Supporting Information).[18]

UV−Vis Spectroscopy. UV−vis diffuse reflectance spectra for the indium tellurites were acquired, and the calculated absorption data were obtained by the Kubelka−Munk function.[14] Extrapolating the straight portion of the rising curve to 0 in the (K/S) versus E plots resulted in the start of absorptions at 4.0, 4.0, 3.9, and 3.9 eV for $NaIn(TeO_3)_2$, $KIn(TeO_3)_2$, $RbInTe_3O_8$, and $CsInTe_3O_8$, respectively (see the Supporting Information). The observed resemblance in band gaps for all four compounds could be mainly due to the interactions of Te−O bonds as well as the existing distortions occurring from TeO_3 and TeO_4 groups.

TGA. TGA and PXRD were used in order to study the thermal properties of the reported compounds. Although all four reported materials do not show any significant weight losses from the thermogravimetric analyses diagrams, the powder X-ray diffraction (PXRD) data taken at different temperatures suggest that both $NaIn(TeO_3)_2$ and $KIn(TeO_3)_2$ break down to In_2TeO_6 (PDF 77-2044) and amorphous phases. However, $RbInTe_3O_8$ and $CsInTe_3O_8$ decompose to unknown amorphous phases at higher temperatures. The TGA data along with the PXRD patterns can be found in the Supporting Information.

Cooperative Effect of Cation Size and Te^{4+} Coordination Mode on Framework Geometry. Although the two stoichiometrically equivalent alkali metal indium tellurites, $NaIn(TeO_3)_2$ and $KIn(TeO_3)_2$, consist of same structural building units, namely, InO_6 and TeO_3, they do exhibit different framework structures. Close structural examination suggests that relatively smaller Na^+ cations in $NaIn(TeO_3)_2$ interact more effectively with seven oxide ligands on InO_6 and TeO_3 polyhedra. In other words, Na^+ cations in $NaIn(TeO_3)_2$ prefer small coordination environments attributable to the small ionic size and reside in the 8-MR channel (see Figure 4a). However, relatively larger K^+ cations in $KIn(TeO_3)_2$ contact eight oxide ligands on other polyhedra and demand a larger space. Thus, K^+ cations occupy the 12-MR channel generated by the corner-

dx.doi.org/10.1021/ic502108a | Inorg. Chem. 2014, 53, 11328−11334

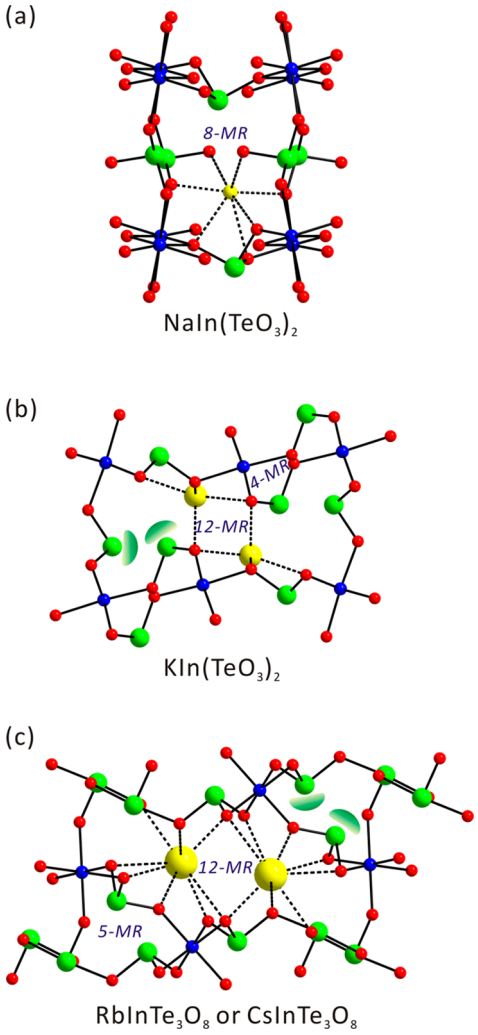

Figure 4. Ball-and-stick representations of the channel structures in (a) $NaIn(TeO_3)_2$, (b) $KIn(TeO_3)_2$, and (c) $RbInTe_3O_8$ or $CsInTe_3O_8$ (blue, In; green, Te; yellow, Na, K, Rb, or Cs; red, O). The lone pair on Te^{4+} is drawn schematically and is not the result of the electron localization function (ELF) calculations.

shared InO_6 and TeO_3 polyhedra (see Figure 4b). Furthermore, the larger alkali metal cations, Rb^+ and Cs^+, in $RbInTe_3O_8$ and $CsInTe_3O_8$ contact nine oxide ligands and require even more space. As seen in Figure 4c, Rb^+ or Cs^+ cations reside in the larger 12-MR channel. It should be noted that, in $KIn(TeO_3)_2$, both of the K^+ cations and the lone pairs on the TeO_3 polyhedra occupy the 12-MR channels (see Figure 4b). However, the lone pairs on Te^{4+} in $RbInTe_3O_8$ and $CsInTe_3O_8$ are found from the outside of the 12-MR channels, because the larger Rb^+ or Cs^+ pushes the lone pairs out in order to prevent unfavorable interactions in the crowded channels of 12-MRs. Instead, the lone pairs on Te^{4+} point within the new 5-MR channels that are obtained by corner-sharings of InO_6, TeO_3, and TeO_4 polyhedra. Compared to $KIn(TeO_3)_2$, a different structural unit, TeO_4, which is a key component for 5-MR, is observed in $RbInTe_3O_8$ and $CsInTe_3O_8$ to maintain the flexible framework structures. In fact, Te^{4+} can form variable coordination modes including TeO_5 square pyramids, TeO_4 seesaws, and TeO_3 trigonal pyramids. Because of the changeable coordination environment of Te^{4+}, a novel framework structure can be achieved. Thus, we can conclude that the cooperative effect of the alkali metal size and the framework flexibility that originates from variable coordination mode of Te^{4+} cation are responsible for the generation of a novel framework structure with 5-MR and 12-MR channels in $RbInTe_3O_8$ and $CsInTe_3O_8$.

Out-of-Center Distortions (Δ_d). The frameworks of the reported alkali metal indium tellurites contain In^{3+} cations with octahedral coordination environments; thus, it would be worthwhile to determine the magnitude of out-of-center distortion for InO_6.[19] Using this methodology, the Δ_d values for InO_6 in $NaIn(TeO_3)_2$, $KIn(TeO_3)_2$, $RbInTe_3O_8$, and $CsInTe_3O_8$ are calculated to be 0.18, 0.11, 0, and 0, respectively. The In^{3+} cation in $NaIn(TeO_3)_2$ or $KIn(TeO_3)_2$ is classified as a weak distorter on the basis of the calculated average Δ_d values.[18] In addition, In^{3+} cations in $RbInTe_3O_8$ and $CsInTe_3O_8$ do not show any distortion at all, since the oxygen ligands move equally to opposite directions. It is not surprising that the In^{3+} cation is categorized as a weak distorter or not a distorter at all, because it is not an SOJT distortive d^0 transition metal cation. Interestingly, however, one can find the relationship between the alkali metal size and the Δ_d values of In^{3+} cations. Relatively smaller cations, Na^+ and K^+, interact strongly with oxide ligands around In^{3+} cations in limited channel structures, which induce slight distortions around the InO_6 octahedra (see Figure 4a,b). The larger cations, Rb^+ and Cs^+, can generate huge channel structures attributable to the large coordination environment, which results in symmetric coordination moieties around the InO_6 octahedra (see Figure 4c).

Dipole Moment Calculations. Since all four reported materials possess polyhedra exhibiting local asymmetric coordination environments, i.e., TeO_3 and/or TeO_4, their distortions can be determined through the dipole moment calculations.[17,20] On the basis of this approach, the calculated dipole moments for TeO_3 and TeO_4 polyhedra in the reported compounds are approximately 8.2−10.1 and 8.3−9.3 D (D = Debyes), respectively. The dipole moments are quite consistent with those previously calculated values for other tellurites.[4g,17,21] A list of dipole moment calculations for the TeO_3 and TeO_4 polyhedra is listed in Table 2.

CONCLUSIONS

Pure samples and single crystals of four quaternary alkali metal indium tellurites, $NaIn(TeO_3)_2$, $KIn(TeO_3)_2$, $RbInTe_3O_8$, and $CsInTe_3O_8$, have been successfully prepared. Although the stoichiometrically similar $NaIn(TeO_3)_2$ and $KIn(TeO_3)_2$ reveal

Table 2. Calculation of Dipole Moments for TeO_3 and TeO_4 Polyhedra

compound	TeO_x	dipole moment (D)[a]
$NaIn(TeO_3)_2$	$Te(1)O_3$	8.3
	$Te(2)O_3$	10.1
$KIn(TeO_3)_2$	$Te(1)O_3$	9.2
	$Te(2)O_3$	8.5
$RbInTe_3O_8$	$Te(1)O_4$	8.3
	$Te(2)O_3$	8.7
	$Te(3)O_3$	8.6
$CsInTe_3O_8$	$Te(1)O_4$	9.2
	$Te(2)O_3$	8.2
	$Te(3)O_3$	8.3

[a]D = Debyes.

dx.doi.org/10.1021/ic502108a | Inorg. Chem. 2014, 53, 11328−11334

3D frameworks composed of InO_6 and TeO_3 polyhedra, they reveal different channel structures attributable to the distinct interactions between alkali metals and oxide ligands. Isostructural $RbInTe_3O_8$ and $CsInTe_3O_8$ show other 3D frameworks consisting of InO_6, TeO_3, and TeO_4 groups, in which the observed flexible backbones may be due to the cooperative influence of alkali metal size and Te^{4+} cation with variable coordination environment. IR and UV−vis diffuse reflectance spectroscopies, elemental analyses, and thermal analyses have been performed. Out-of-center distortions and dipole moment calculations for the new materials have been also reported.

■ ASSOCIATED CONTENT

Supporting Information

X-ray crystallographic file in CIF format, calculated and observed XRD patterns, TGA diagrams, IR spectra, and UV−vis diffuse reflectance spectra for $NaIn(TeO_3)_2$, $KIn(TeO_3)_2$, $RbInTe_3O_8$, and $CsInTe_3O_8$. This material is available free of charge via the Internet at http://pubs.acs.org.

■ AUTHOR INFORMATION

Corresponding Author

*E-mail: kmok@cau.ac.kr. Phone: +82-2-820-5197. Fax: +82-2-825-4736.

Notes

The authors declare no competing financial interest.

■ ACKNOWLEDGMENTS

This research was supported by the Chung-Ang University Freshmen Academic Record Excellent Scholarship Grants in 2014 (for S.-w.B.). This research was also supported by the National Research Foundation of Korea (NRF) funded by Ministry of Science, ICT and Future Planning (Grant 2013R1A2A2A01007170).

■ REFERENCES

(1) Cotton, F. A.; Wilkinson, G. *Advanced Inorganic Chemistry*, 2nd ed.; Interscience: New York, 1966.

(2) West, A. R. *Solid State Chemistry and Its Applications*; John Wiley & Sons: New York, 1984.

(3) (a) Alonso, J. A.; Castro, A.; Puebla, E. G.; Monge, M. A.; Rasines, I.; Valero, C. R. *J. Solid State Chem.* **1987**, *69*, 36−42. (b) Champarnaud-Mesjard, J. C.; Frit, B.; Chagraoui, A.; Tairi, A. *J. Solid State Chem.* **1996**, *127*, 248−255. (c) Ok, K. M.; Orzechowski, J.; Halasyamani, P. S. *Inorg. Chem.* **2004**, *43*, 964−968. (d) *CRC Handbook of Chemistry and Physics, Internet Version 2005*; Lide, D. R., Ed.; CRC Press: Boca Raton, FL, 2005.

(4) (a) Alcock, N. W.; Harrison, W. D. *Acta Crystallogr.* **1982**, *B38*, 1809−1811. (b) Tagg, S. L.; Huffman, J. C.; Zwanziger, J. W. *Chem. Mater.* **1994**, *6*, 1884−1889. (c) Tagg, S. L.; Huffman, J. C.; Zwanziger, J. W. *Acta Chem. Scand.* **1997**, *51*, 118−121. (d) Mayer, H.; Weil, M. *Z. Anorg. Allg. Chem.* **2003**, *629*, 1068−1072. (e) Kong, F.; Hu, C.; Hu, T.; Zhou, Y.; Mao, J.-G. *Dalton Trans.* **2009**, 4962−4970. (f) Kim, M. K.; Kim, S.-H.; Chang, H.-Y.; Halasyamani, P. S.; Ok, K. M. *Inorg. Chem.* **2010**, *49*, 7028−7034. (g) Kim, Y. H.; Lee, D. W.; Ok, K. M. *Inorg. Chem.* **2014**, *53*, 5240−5245.

(5) (a) Opik, U.; Pryce, M. H. L. *Proc. R. Soc. London* **1957**, *A238*, 425−447. (b) Bader, R. F. W. *Can. J. Chem.* **1962**, *40*, 1164−1175. (c) Pearson, R. G. *J. Am. Chem. Soc.* **1969**, *91*, 4947−4955. (d) Pearson, R. G. *THEOCHEM* **1983**, *103*, 25−34. (e) Wheeler, R. A.; Whangbo, M.-H.; Hughbanks, T.; Hoffmann, R.; Burdett, J. K.; Albright, T. A. *J. Am. Chem. Soc.* **1986**, *108*, 2222−2236.

(6) (a) Nye, J. F. *Physical Properties of Crystals*; Oxford University Press: Oxford, 1957. (b) Jona, F.; Shirane, G. *Ferroelectric Crystals*; Pergamon Press: Oxford, 1962. (c) Cady, W. G. *Piezoelectricity: An Introduction to the Theory and Applications of Electromechanical Phenomena in Crystals*; Dover: New York, 1964. (d) Lang, S. B. *Sourcebook of Pyroelectricity*; Gordon & Breach Science: London, 1974. (e) Ok, K. M.; Chi, E. O.; Halasyamani, P. S. *Chem. Soc. Rev.* **2006**, *35*, 710−717.

(7) (a) Philippot, E.; Astier, R.; Loeksmanto, W.; Maurin, M.; Moret, J. *Rev. Chim. Miner.* **1978**, *15*, 283−291. (b) Lee, D. W.; Oh, S.-J.; Halasyamani, P. S.; Ok, K. M. *Inorg. Chem.* **2011**, *50*, 4473−4480. (c) Lee, D. W.; Ok, K. M. *Inorg. Chem.* **2013**, *52*, 6236−6238.

(8) (a) Gaudin, E.; Chaminade, J. P.; El Abed, A.; Darriet, J. *Acta Crystallogr., Sect. C* **2001**, *C57*, 1004−1005. (b) Boukharrata, N. J.; Laval, J. P.; Thomas, P. *Acta Crystallogr., Sect. C* **2008**, *C64*, i53−i56. (c) Ajaz, H.; Deiseroth, H. J.; Schlosser, M.; Rabbani, F. *Synth. React. Inorg., Met.-Org., Nano-Met. Chem.* **2009**, *39*, 209−210. (d) Jennene Boukharrata, N.; Laval, J. P. *J. Alloys Compd.* **2011**, *509*, 1517−1522. (e) Jennene Boukharrata, N.; Duclere, J.-R.; Laval, J.-P.; Thomas, P. *Acta Crystallogr., Sect. C* **2013**, *C69*, 460−462.

(9) *SAINT, Program for Area Detector Absorption Correction, version 4.05*; Siemens Analytical X-ray Instruments: Madison, WI, 1995.

(10) Blessing, R. H. *Acta Crystallogr., Sect. A* **1995**, *A51*, 33−38.

(11) Sheldrick, G. M. *SHELXS-97—A Program for Automatic Solution of Crystal Structures*; University of Goettingen: Goettingen, Germany, 1997.

(12) Sheldrick, G. M. *SHELXL-97—A Program for Crystal Structure Refinement*; University of Goettingen: Goettingen, Germany, 1997.

(13) Farrugia, L. J. *J. Appl. Crystallogr.* **1999**, *32*, 837−838.

(14) (a) Kubelka, P.; Munk, F. *Z. Tech. Phys.* **1931**, *12*, 593. (b) Tauc, J. *Mater. Res. Bull.* **1970**, *5*, 721−729.

(15) (a) Brown, I. D.; Altermatt, D. *Acta Crystallogr.* **1985**, *B41*, 244−247. (b) Brese, N. E.; O'Keeffe, M. *Acta Crystallogr.* **1991**, *B47*, 192−197.

(16) Lee, D. W.; Kim, S. B.; Ok, K. M. *Inorg. Chem.* **2012**, *51*, 8530−8537.

(17) Galy, J.; Meunier, G. *J. Solid State Chem.* **1975**, *13*, 142−159.

(18) (a) Dimitriev, Y.; Dimitrov, V.; Arnaudov, M. *J. Mater. Sci.* **1983**, *18*, 1353−1358. (b) Charton, P.; Gengembre, L.; Armand, P. *J. Solid State Chem.* **2002**, *168*, 175−183. (c) Lee, D. W.; Oh, S. J.; Halasyamani, P. S.; Ok, K. M. *Inorg. Chem.* **2012**, *50*, 4473.

(19) Halasyamani, P. S. *Chem. Mater.* **2004**, *16*, 3586−3592.

(20) (a) Maggard, P. A.; Nault, T. S.; Stern, C. L.; Poeppelmeier, K. R. *J. Solid State Chem.* **2003**, *175*, 27−33. (b) Izumi, H. K.; Kirsch, J. E.; Stern, C. L.; Poeppelmeier, K. R. *Inorg. Chem.* **2005**, *44*, 884−895.

(21) Kim, Y. H.; Lee, D. W.; Ok, K. M. *Inorg. Chem.* **2014**, *53*, 1250−1256.